Bidirectional Control of Sphingomyelinase Activity and Surface Topography in Lipid Monolayers

María Laura Fanani, Steffen Härtel, Rafael G. Oliveira, and Bruno Maggio

Departamento de Química Biológica, Facultad de Ciencias Químicas, Universidad Nacional de Córdoba, Ciudad Universitaria, 5000 Córdoba, Argentina

ABSTRACT Lipid lateral organization is increasingly found to modulate membrane-bound enzymes. We followed in real time the reaction course of sphingomyelin (SM) degradation by *Bacillus cereus* sphingomyelinase (SMase) of lipid monolayers by epifluorescence microscopy. There is evidence that formation of ceramide (Cer), a lipid second messenger, drives structural reorganization of membrane lipids. Our results provide visual evidence that SMase activity initially alters surface topography by inducing phase separation into condensed (Cer-enriched) and expanded (SM-enriched) domains. The Cer-enriched phase grows steadily as the reaction proceeds at a constant rate. The surface topography derived from the SMase-driven reaction was compared with, and found to differ from, that of premixed SM/Cer monolayers of the same lipid composition, indicating that substantial information content is stored depending on the manner in which the surface was generated. The long-range topographic changes feed back on the kinetics of Smase, and the onset of condensed-phase percolation is temporally correlated with a rapid drop of reaction rate. These observations reveal a bidirectional influence and communication between effects taking place at the local molecular level and the supramolecular organization. The results suggest a novel biocatalytic-topographic mechanism in which a surface enzymatic activity can influence the function of amphitropic proteins important for cell function.

INTRODUCTION

There is strong evidence that lipid organization can modulate the interaction of peripheral (amphitropic) proteins with membrane surfaces. An intimate coupling between chemical composition, physical state, domain formation, surface pressure, electrostatic potential, interfacial curvature, and function has been postulated (Kinnunen et al., 1994). Phospholipases are a group of enzymes that act as peripheral membrane proteins whose activity can be controlled by noncovalent binding to lipids. It is well established that both the long-range physical state and the fine intermolecular organization of the phospholipid substrate markedly affect the activity of several phospholipases from different sources (Ransac et al., 1991; Maggio, 1996; Honger et al., 1997). Currently, almost all phosphohydrolytic enzymes known so far are thought to be involved in some sort of membrane-mediated signal transduction (Exton, 1994; Hannun and Luberto, 2000). These enzymes are represented by a rather heterogeneous group of proteins (Roberts, 1996). However, despite their structural diversity, the activity of each individual enzyme against a phospholipid surface depends only on the variation of a few generic interfacial parameters. Intermolecular packing, phase state, and dipole potential regulate the phosphohydrolytic activities within a relatively narrow range of values (Wakelam et al., 1993; Kinnunen et al., 1994; Boguslavsky et al., 1994; Volwerk et al., 1994; Maggio, 1996, 1999; Fanani and Maggio, 1997, 1998).

The best studied members of phospholipases in terms of their structural features and of their regulation by the lateral organization of the phospholipid belong to the secretory and venom phospholipases A_2 (PLA_2) (Bianco et al., 1991; Maggio et al., 1994; Berg et al., 1997; Honger et al., 1997). PLA_2 reaches its maximum activity in the range of temperature where the gel-to-liquid phase transition of the phospholipid substrate takes place (Op den Kamp et al., 1975; Honger et al., 1997). Under these conditions, a coexistence of clusters in two different physical states is established, which introduces lateral defects in the organization of the lipid packing. These defects enhance the PLA_2 activity mainly by increasing enzyme penetration and substrate availability (Jain et al., 1986). Epifluorescence visualization of PLA_2 action against lipid monolayers revealed that activation is initiated at the boundary of the gel-liquid crystalline domains (Grainger et al., 1990) providing direct evidence that lateral defects favor penetration of this enzyme.

In an analogous manner, lateral separation and domain formation originated by the addition of nonsubstrate molecules induces activation of PLA_2 (Bell et al., 1996). All these results agree with the mechanism proposed to explain the presence of a latency period for PLA_2 activity in lipid bilayers (Burack et al., 1993). In the latter, the burst of activity at the end of the lag time is promoted by lateral domain separation produced when the enzymatic lipid products (lysophospholipid and fatty acid) reach a defined concentration threshold. Pancreatic lipase activity has been reported to be regulated by dynamic lipid lateral organization, and formation of substrate domains regulates the adsorption of colipase to a PC-enriched monolayer (Sugar et

Submitted June 12, 2002, and accepted for publication July 29, 2002.

Address reprint requests to Dr. Bruno Maggio, Departamento de Química Biológica-CIQUIBIC, Facultad de Ciencias Químicas, Universidad Nacional de Córdoba, Ciudad Universitaria, 5000 Córdoba, Argentina. Tel.: 054-351-4334168; Fax: 054-351-4334074; E-mail: bmaggio@dqb.fcq.unc.edu.ar.

0006-3495/02/12/3416/09 $2.00

al., 2001). In a similar system the connection-disconnection of statistically distributed substrate domains modulate pancreatic lipase-efficient adsorption and activity (percoregulation) (Muderhwa and Brockman, 1992).

Recently, attention has been focused on the degradative pathways of sphingomyelinases (SMases), which hydrolyze the membrane constituent sphingomyelin (SM) to phosphocholine and ceramide (Cer). Although Cer in its function as a second messenger has been investigated intensively for many years, there is growing evidence for a pivotal role of the conversion SM→Cer to drive basic structural reorganization in lipid membranes. Enhancement of membrane permeabilization, the induction of membrane fusion (Ruiz-Arguello et al., 1996), small lipid vesicle formation at the surface of giant liposomes (Holopainen et al., 2000), and the generation of apoptotic bodies during cellular apoptosis were linked causally to the SM→Cer conversion (Tepper et al., 2000). In model membranes, an increasing concentration of Cer produced by bacterial SMase in one-half of the lipid bilayer leads to the formation of Cer-enriched domains, which consecutively bend the bilayer because of the inverted cone-like shape of Cer (Holopainen et al., 2000). Cer-enriched domains with a pronounced tendency to form nonbilayer lipid phases also modulate the activity of protein kinase C (Huang et al., 1999). This cell-signaling key enzyme activity is activated by interaction with lipid interfaces and strongly influenced by its physical organization (Souvignet et al., 1991). On the other hand, the depletion of SM in combination with an associated rupture of SM-cholesterol clusters in cellular membranes can force morphological changes leading to bilayer bending and vesicle shedding (Tepper et al., 2000).

Fluorometric studies strongly support that asymmetric enzymatic generation of Cer in phospholipid bilayers leads to surface reorganization in the form of lateral phase separation (Holopainen et al., 1998). Based on the different cross-sectional area of SM and Cer in lipid monolayers we previously showed that the activity of *Bacillus cereus* SMase can be followed in real time under precisely controlled substrate organization and described the preferential degradation of SM monolayers in the liquid-expanded state (Fanani and Maggio, 1997, 1998). A recent publication also showed preference of SMase for fluid-state bilayer vesicles (Ruiz-Arguello et al., 2002). Our previous studies also allowed the description of a latency time before SMase reaches its maximum activity against monolayers (Fanani and Maggio, 1997). This lag time involves interfacial partition at the interface and a bimolecular enzyme-dependent step followed by a slow irreversible rate-limiting enzymatic activation (Fanani and Maggio, 2000). After the lag time, the enzymatic activity reaches a steady-state regime (pseudo-zero-order kinetics), subsequently followed by a gradual halting of product formation.

In the present work we show for the first time how *B. cereus* SMase activity perturbs the surface topography of SM monolayers by following the reaction course of the degradation of SM by *B. cereus* SMase with epifluorescence microscopy using the preferential partition of the fluorescent probe 1,1′-didodecyl-3,3,3′,3′-tetramethylindocarbocyanine ($DiIC_{12}$) into the liquid-expanded (LE) phase of the monolayer. This allows real-time visualization of the formation of laterally separated phase domains while, at the same time, the intermolecular organization in terms of parameters such as surface pressure and average molecular area is precisely controlled. Basic topographic parameters of the evolving surface pattern were derived by interactive image-processing routines, leading to a direct time-dependent quantitative exploration of the topographical features caused by the enzymatic reaction. Finally, we compare the lipid organization emerging from the SMase-driven process with that exhibited by enzyme-free, mixed monolayers of SM/Cer at a similar composition.

MATERIALS AND METHODS

Chemicals

Bovine brain SM was purchased from Avanti Polar Lipids (Alabaster, AL). *B. cereus* SMase (lot 48H4058) and Cer type III (from bovine brain SM) were obtained from Sigma-Aldrich (St. Louis, MO). The lipophilic fluorescent probe $DiIC_{12}$ was purchased from Molecular Probes (Eugene, OR). Solvents and chemicals were of the highest commercial purity available, and NaCl was roasted at 500°C for 4 h. Absence of surface-active impurities in the solvents and buffers was routinely checked as described previously (Maggio et al., 1994).

Epifluorescence microscopy of monolayers

SM/$DiIC_{12}$ and SM/Cer/$DiIC_{12}$ monolayers (0.5 mol % $DiIC_{12}$ was incorporated into the lipid solution before spreading) were obtained by spreading 20 μl of lipid solution in chloroform/methanol (2:1) over a subphase of 10 mM Tris/HCl, 125 mM NaCl, 3 mM $MgCl_2$, pH 8, until reaching a surface pressure of ~0.5 mN/m (Fanani and Maggio, 1997). After the solvent was allowed to evaporate for 10 min, the monolayer was slowly compressed to the desired pressure. For monolayer equilibration, 15 min were allowed after the desired surface pressure was reached. The observations were carried out at room temperature, using an all-Teflon zero-order trough (Kibron μ Trough S, Kibron, Helsinki, Finland). An open-end Teflon mask with a lateral vertical slit (covering the objective and extending through the film into the subphase) was used to restrict lateral monolayer flow under the field being observed. A Zeiss Axioplan (Carl Zeiss, Oberkochen, Germany) epifluorescence microscope with a source of UV radiation provided by a mercury lamp HBO 50, an objective of ×20, and a rhodamine filter set was used. Images (exposure times between 0.1 and 0.3 s) were registered by a CCD video camera (Micromax, Princeton Instruments, Downingtown, PA) commanded through Metamorph 3.0 software (Universal Imaging Corp., PA).

Determination of enzymatic activity

The enzymatic reaction was followed in real time after injection of a diluted solution of SMase into the subphase of the reaction compartment (2 ml; 3.14 cm^2) to reach a bulk concentration of 228 pmol/ml. The reaction compartment consists of a circular trough with an adjacent reservoir compartment, connected through a narrow and shallow slit to the substrate

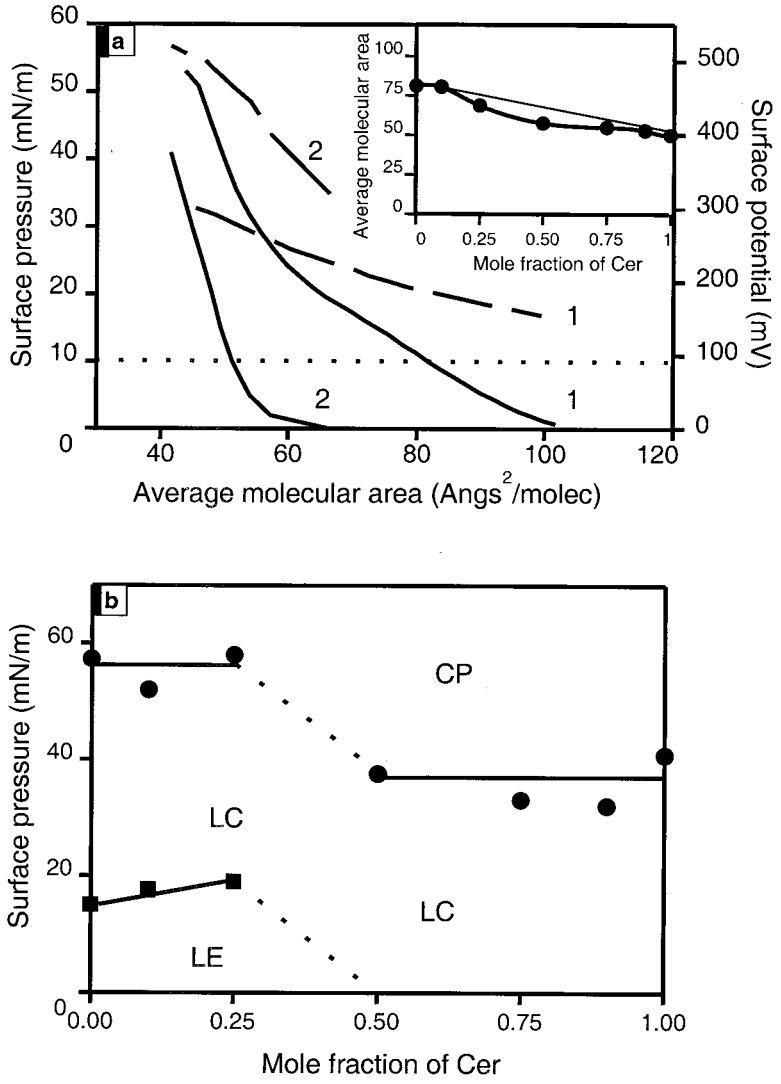

FIGURE 1 Characterization of surface properties of sphingomyelin (SM) and ceramide (Cer) in pure and mixed lipid monolayers at the air-water interface. (*a*) Surface pressure (——) and surface potential (— — —) molecular area isotherms of SM (*1*) and Cer (*2*). A surface pressure of 10 mN/m (· · ·) was routinely used for the enzymatic assay. The inset shows the average molecular area of mixed SM/Cer monolayer as a function of Cer mole fraction at 10 mN/m. (*b*) Two-dimensional phase diagram of SM/Cer mixed monolayers. CP, collapsed-phase region.

monolayer, and an automated surface barostat. A constant lateral surface pressure (10 mN/m) was maintained by replenishment from the reservoir compartment with a film of pure SM (Fanani and Maggio, 1997). By periodically controlled visualization of the monolayer on the reservoir compartment we ascertained that the latter remained uncontaminated by lateral diffusion of product and kept the properties of a pure SM monolayer (see Fig. 2 *a*). The time course for the SMase-driven enzymatic conversion of SM to Cer in lipid monolayers was determined by recording the reduction of the surface area by the film barriers of the surface balance to maintain a constant surface pressure (Fanani and Maggio, 1997). This technique is based on the different cross-sectional molecular surface area of SM and the reaction product Cer in monolayers (Fig. 1 *a*).

Computational analysis of surface topography

At 10 mN/m, the monolayers of SM is LE, whereas Cer-enriched films form liquid-condensed (LC) monolayers (see Fig. 1 *b*). The lipophilic fluorescent probe $DiIC_{12}$ shows preferential partition in the LE phase of the lipid monolayer (Spink et al., 1990). In the images recorded, segmentation of $DiIC_{12}$-depleted areas was archived by interactive image processing routines written in IDL (Interactive Data Language, Research Systems Co., Boulder, CO). After applying a gradient filter to correct images for smear produced by the Micromax CCD camera system, LE and LC lipid phases are represented homogeneously by bright (high-fluorescence/$DiIC_{12}$-enriched) and dark (low-fluorescence/$DiIC_{12}$-depleted) pixels in the 8-bit image intensity (I) interval ($I \in (0,255)$; see Figs. 2 and 4). The separation of bright and dark regions into binary object masks for the Cer- and SM-enriched domains was achieved by a combination of boundary detection filters followed by a successive treatment of pixel erosion and dilatation operations (Ellison and Castellino, 1997). The quality of the segmentation was optimized interactively by overlaying the calculated object masks with the original fluorescent pictures.

Image-processing routines were also used for the calculation of three basic topographic parameters for Cer-enriched domains. 1) The percentage of monolayer surface covered by Cer-enriched domains was calculated from the surface area (pixels per image) covered by Cer- and by SM-enriched domains in the binary object masks of each of the corresponding images. 2) The number of unconnected Cer-enriched domains per image frame was calculated as follows: the connectivity of object domains in the binary object masks of each image was defined with a four-neighbor searching algorithm. After that, unconnected objects were numbered and counted in the corresponding images. 3) The sum of the borderlines between Cer- and SM-enriched domains per frame was determined with the Freeman-chain code (Freeman, 1970)

used to identify object borders. The length of the chain code borders P was determined for each object by:

$$P = \alpha N_g + \beta N_d + \gamma N_e,$$

where N_g denotes the number of horizontally or vertically connected points in the border chain code, N_d denotes diagonal connectivity, and N_e represents the number of end points. Choosing $\alpha = 0.98$, $\beta = 1.406$, and $\gamma = -0.091$, Vossepoel and Smeulders (1982) report that object borders are estimated with a precision of ~99%.

RESULTS AND DISCUSSION

Although the compression isotherm of SM shows a LE-to-LC phase transition at ~15 mN/m, the compression isotherm of Cer ranging from 4 mN/m to the collapse point at 40 mN/m remains highly condensed (Fig. 1 *a*). Monolayers of both lipids in different proportions reveal ideal behavior and follow the additivity rule at high surface pressure for the mean molecular area as well as for the mean surface (dipole) potential per unit of molecular surface density. As can be seen in Fig. 1 *b*, the isobaric collapse and transition pressure is independent of the lipid composition. This indicates that Cer and SM are rather immiscible in the monomolecular film at high pressures. Nevertheless, at the lower surface pressure used in our study, the mean molecular parameters show small deviations from the ideal behavior by 5–12% (Fig. 1 *a*, *inset*), indicating some miscibility.

SMase-driven changes of surface topography

Direct visual evidence for SMase-induced phase separation is provided by epifluorescence microscopy with the fluorescent membrane dye $DiIC_{12}$. Time sequence analysis of the enzymatic reaction reveals that $DiIC_{12}$ distributes rather uniformly in the pure SM film (some defects, seen as irregularly arranged dark spots in Fig. 2 *a*, represent less than 3% of the surface area). On the other hand, $DiIC_{12}$ does not partition into monolayers of pure Cer, showing an almost homogeneously dark image with few highly scattered very brilliant spots of nearly pure dye (not shown). As a function of time, progressive enzymatic generation of Cer by the action of SMase leads to the formation of laterally segregated condensed phase domains, which exclude the fluorescent probe (Fig. 2, *b–g*). In this manner, Cer is segregated from the LE phase and does not alter the enzymatic rate (Fanani and Maggio, 1998). During the lag time (~2.5 min), the number of dark domains increases up to the beginning of the period of zero-order kinetics (Fanani and Maggio, 1997). At this point, the number of domains levels off at 550–600 domains/frame, and the mean domain size increases in an approximately linear manner (Fig. 3). The pattern distribution of domains is quite regular over the long range (5–10 μm) and shows a defined superstructural arrangement in terms of the separation distances between domains (Fig. 2, *c–f*). At a Cer concentration near 70%, the percolation threshold of the dark domain phase is reached. The condensed phase becomes continuous, and disconnection of the expanded phase takes place (Fig. 2, *g* and *h*). At this point, the mean size of dark domains is significantly increased, and both the number of domains/frame and the border length of the lateral interface are decreased abruptly (Fig. 3 *b*).

Feedback influence of surface topography on SMase activity

Changes of basic topographical parameters of the surface domains of the monolayer appear to correlate reciprocally with changes in the course of the enzymatic activity. The comparison between the analysis of epifluorescence images and the kinetic results indicate that during the lag time, new segregated domains appear on the SM surface. This is evidenced by an increase in the number of dark clusters and a concomitant fast increase of the border length of the lateral phases (Fig. 3, *a* and *b*). During this period, the reaction rate is continuously increasing as we have previously shown in a detailed analysis (Fanani and Maggio, 2000). During the second phase (2.5–4.5 min) the reaction shows a constant rate (pseudo-zero-order kinetic behavior due to relative substrate excess), the number of domains remains rather constant, and the border length of the lateral interfaces reaches its maximum. As the reaction proceeds, the percolation threshold is reached in ~4.6 min. This event coincides with the deviation of the reaction from the pseudo-zero-order kinetics and rapid drop of SM hydrolysis at ~70% degradation.

Topographical comparison between SMase-degraded and premixed monolayers

As can be seen in Fig. 4, the surface topography of monolayers generated by spreading from premixed solutions of SM/Cer is markedly different from that of enzymatically generated films at the same SM/Cer proportions. Compared with the surface topography generated by the enzymatic reaction, it can be observed that the premixed interface generally contains a significantly larger proportion of condensed phase (Figs. 4 and 5) and that lateral percolation occurs at a lower percentage of Cer (at ~25 mol %; Fig. 5) than in the monolayer altered by the enzymatic activity (~70 mol %; Fig. 3). In both cases, the percolation is evidenced by a significant decrease in the number of domains/frame (Fig. 5). Additionally, detailed topographical features of both monolayers in both conditions close to the percolation threshold are substantially different. In the percolation occurring in premixed films, condensed rounded domains are first lined up and then become connected by merging of fused rows that progressively interlink and finally form nested structures (Fig. 5, *upper left inset*) as the propor-

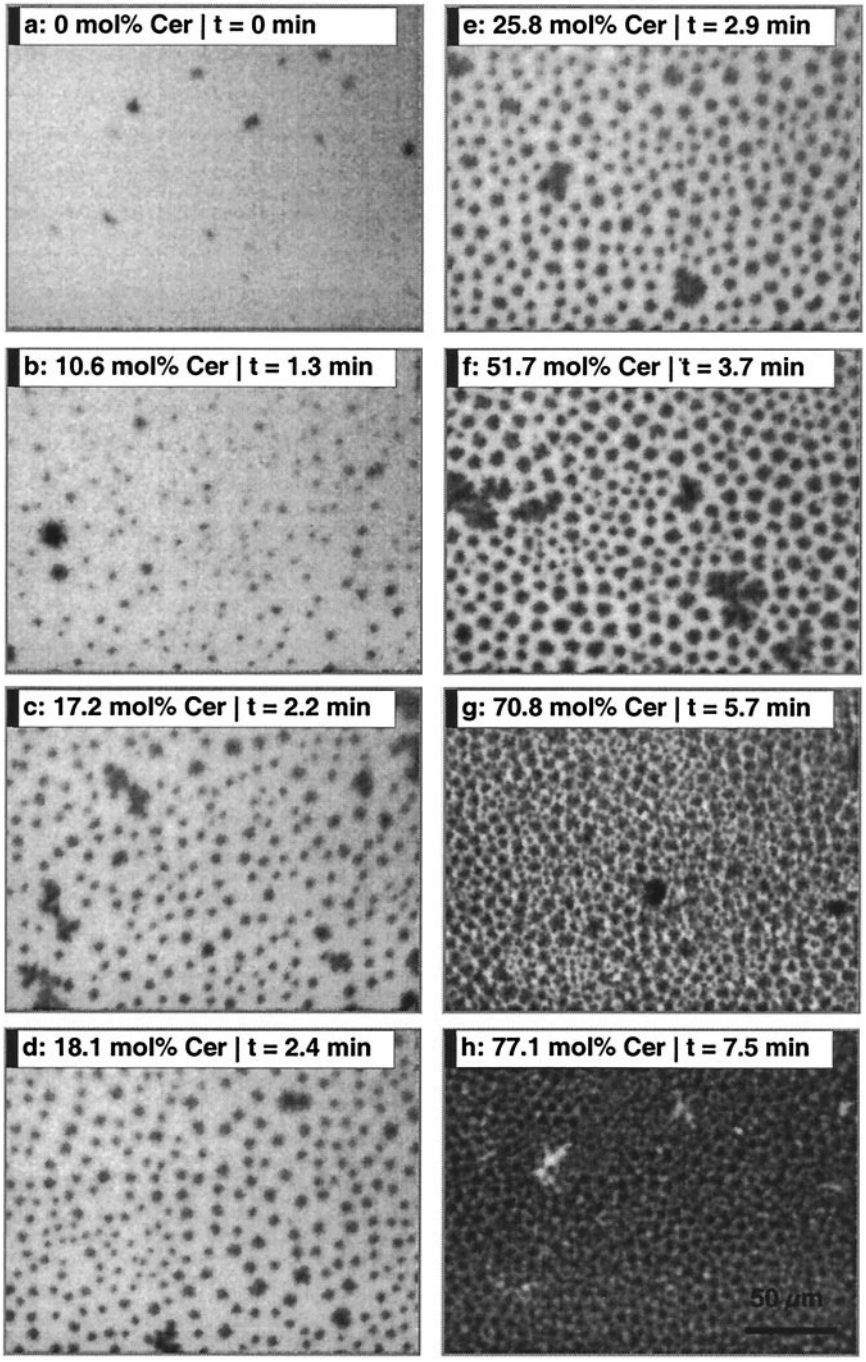

FIGURE 2 Time course of Smase-driven conversion of SM to Cer in lipid monolayers at 10 mN/m. (*a–h*) Representative pictures of $DiIC_{12}$ fluorescence in SM/Cer monolayers at different times of the enzymatic reaction. Dark regions in the pictures represent the formation of Cer-enriched lipid phases with unfavorable partition conditions for the lipophilic fluorescent probe $DiIC_{12}$.

tion of Cer increases. When Cer is generated enzymatically, the percolation occurs by connection of small regular sized star-like condensed domains (Fig. 5, *upper right inset*).

The results show that on a first supramolecular level, the organization of lateral lipid domains depends on how the mixture was generated locally. Especially at low Cer concentrations ($\leq$10 mol %), $DiIC_{12}$-depleted domains formed in the premixed interface cover an area whose relatively large coverage cannot be accounted for a phase of pure Cer (Figs. 4 and 5). In keeping with the partial miscibility of SM and Cer at 10 mN/m (see Fig. 1), these domains should contain a significant fraction of SM molecules but still maintain a relatively high condensed state with unfavorable partition conditions for $DiIC_{12}$. On the other hand, the area of the $DiIC_{12}$-depleted domains formed by SMase activity probably represents highly enriched phases of Cer (as preliminary calculations suggest), rapidly formed locally by the enzyme, largely excluding SM.

On a second level of organization, the different composition of the $DiIC_{12}$-depleted domains leads to a different phase topography (note the dominating rounded shape of

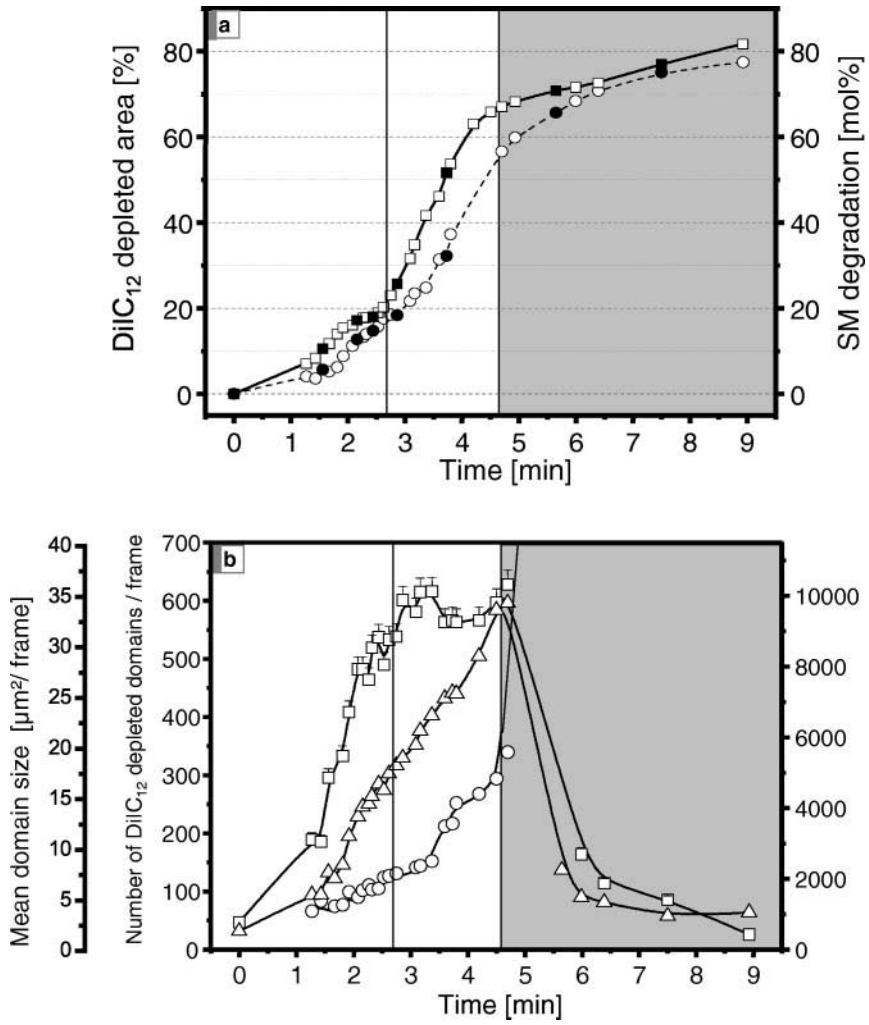

FIGURE 3 Quantitative evaluation of Cer-enriched domains during the time course of Smase-driven conversion of SM to Cer. (*a*) Time-dependent separation of lipid phases and SM degradation due to SMase-driven SM→Cer conversion. ○- - -, $DiIC_{12}$-depleted areas as segmented in the fluorescent picture series; □——, SM degradation as calculated from the reduction of the total film area by the surface barrier movement of the barostat at constant surface pressure; ● and ■, points for which selected pictures are shown in Fig. 2, *a–h*. For all plots, data points were connected by b-spline curves. SEMs are within the size of the symbols. (*b*) Mean size (○), number of $DiIC_{12}$-depleted areas (□), and total domain borderline (△) per frame as derived by segmentation of Cer-enriched domains from the CCD picture series. The size of the frames used for calculation is 177 × 225 μm (see Fig. 2). In both plots, the vertical line at the left marks the end of the lag time. The light gray region on the right marks the end of the zero-order kinetics of the reaction that coincides with the initiation of fusion between individual Cer-enriched domains, resulting in the formation of a rigid Cer lattice.

the domains formed in the premixed interface and the fingered structure of many domains formed by SMase activity in Fig. 4). The different composition and structure of the domains also induce percolation at quite different Cer concentrations, and the maximum number of $DiIC_{12}$-depleted domains just before percolation is ~30% higher for the premixed interface (Fig. 5). Interestingly, the surface area covered by the domains just before percolation for both generation processes is quite similar (~46% for the pre-mixture and ~50% for Smase; Fig. 5). Consequently, the average Cer-enriched domain size before percolation is significantly smaller in the case of the pre-mixture (compare Fig. 2 *f* with Fig. 4 *i*).

Finally, on a third level of organization, domains formed by SMase activity seem to adopt a flexible but visually perceptible super-lattice structure at Cer concentrations of ~50 mol % (Fig. 2 *f*). Hexagonal lattice arrangement and Cer domains organized like pearl necklaces can be found quite frequently in the lattice-like organization of the domains. A domain organization of such nature is not found for domains generated in the premixed films at any Cer concentration.

Summing up the phenomena described above, our observations disclose a remarkable amplification on the supramolecular level of the biocatalytic reaction. We observe consecutive ordering phenomena, ranging from the local molecular level (Cer formation) to a topographical level (Cer segregation with domain formation) up to a long-range super-lattice organization of the domains. These transduction processes convey information derived from time-dependent compositional changes of the interface (modulated enzyme kinetics) through different interfacial levels up to the surface organization on a micrometer scale.

Cer segregation and domain formation

So far, evidence for Cer segregation and domain formation in two-dimensional lipid organization has been described in liposomes, combining fluorescent techniques to determine lipid aggregation (excimer formation between pyrene labeled lipids) and microviscosity changes (rotational diffusion of diphenylhexatriene) with calorimetric studies (Hol-

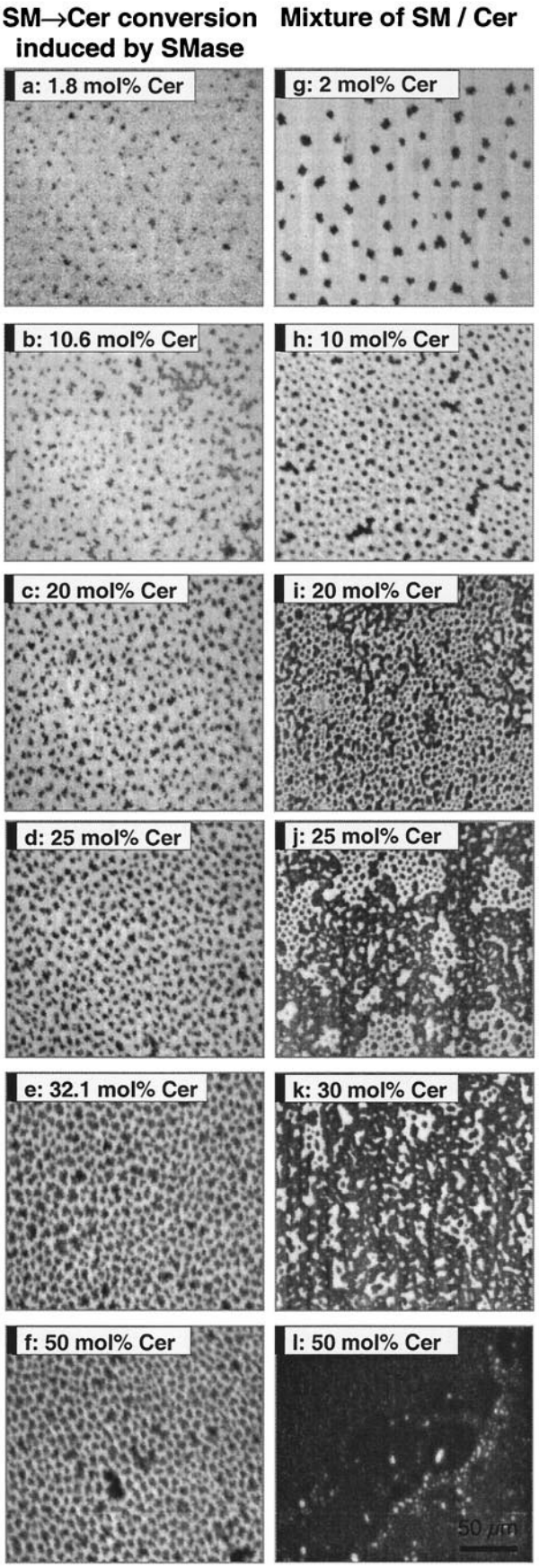

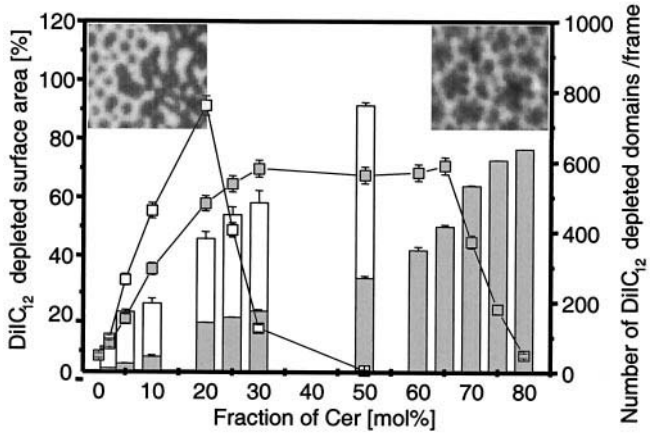

FIGURE 5 Comparative kinetic and topographic quantification of the formation of Cer-enriched lipid domains as observed in SMase-driven SM-Cer conversion and in defined mixtures of SM/Cer. Columns represent $DiIC_{12}$-depleted lipid surface area as derived by segmentation of Cer-enriched domains (see Fig. 4). The gray columns represent SMase-driven SM→Cer conversion; the white columns represent premixed films of SM/Cer. The numbers of $DiIC_{12}$-depleted domains per frame are shown for the SMase-driven SM→Cer conversion (*gray squares*) and for the premixed monolayer of SM/Cer (*white squares*). The insets show amplifications of Cer-enriched domains during percolation. The upper left inset corresponds to premixed films of SM/Cer at 25 mol % Cer (Fig. 4 *j*); the upper right inset corresponds to enzymatically generated films of SM/Cer at 70.8 mol % Cer (Fig. 2 *g*).

opainen et al., 1997). By these methods, the formation of a distinct Cer-enriched phase could be detected in binary membranes of dimyristoylphosphatidylcholine and natural Cer at proportions exceeding 10 mol %. In DPPC bilayers, phase separation could already be detected in a range between 1 and 5 mol % Cer (Carrer and Maggio, 1999). In this paper, we provide direct visual evidence of Cer segregation and extensive domain formation in SM monolayers covering ~15% of the surface area, starting at Cer concentrations as low as 2 mol % (Fig. 4 *g*).

Segregation of C16:0-Cer and domain formation in palmitoyl-oleoyl-phosphatidylcholine/C16:0-SM liposomes occurs as a result of SM→Cer conversion by SMase. Fast SM→Cer conversion (85% after 3 min at 30°C) was accompanied by a fast decrease of the rotational diffusion of DPH, but increase of excimer formation between pyrene-labeled Cer was significantly slower (almost 2 h to reach steady state) (Holopainen et al., 1998), indicating a slow reorganization of Cer into specific microdomains. Conversely, in our experimental setup, $DiIC_{12}$ redistribution occurred simultaneously with the SMase-in-

FIGURE 4 Evolution of Cer-enriched domains during the time course of sSMase-driven conversion of SM to Cer (*left column*) and the formation of Cer-enriched domains spread as a defined mixture of SM/Cer in lipid monolayers (*right column*). Epifluorescence pictures, using the lipophilic fluorescent probe $DiIC_{12}$, were taken at 10 mN/m. All frames represent a size of 177 × 225 μm.

duced SM→Cer conversion as determined by surface barrier movement (Fig. 3 *a*), indicating a rapid formation of Cer-enriched domains. The direct visualization of a fast Cer domain formation contributes evidence to support that a rapid SMase-induced formation of Cer can enhance solute efflux from liposomes (Montes et al., 2002) or its implication in vectorial budding of lipid vesicles from giant liposomes (Holopainen et al., 2000).

Bottom-up and top-down transduction of information

The fact that the surface topography at different levels of lipid organization can depend dramatically on how the lipid composition is generated in situ might provide a solid basis to explain recent findings in which membrane permeability differed significantly, depending just on the way Cer was incorporated into these membranes (Montes et al., 2002). These findings at the macroscopic level fully agree with our bottom-up line of argument that successive transduction of information through organization from a molecular level to a mesoscopic level leads to a redefinition of membrane parameters and thus membrane function.

Vice versa, a line of arguments propagating a top-down signal transduction from long-range membrane properties down to individual molecules with regulative power on its function has already been established successfully for PLA_2. It was well documented that the level of PLA_2 activity was correlated to lateral membrane defects (Jain et al., 1986; Burack et al., 1993), to dynamic structural domain microheterogeneity (Honger et al., 1996), to coexistence of bilayer and nonbilayer phases (Maggio, 1996), and to the presence in the interface of nonsubstrate lipids (Bianco et al., 1991; Maggio et al., 1994; Fanani and Maggio, 1997, 1998) or proteins (Bianco et al., 1992). Additionally, direct visualization of PLA_2 showed its activation at the border of gel-liquid crystalline domains (Grainger et al., 1990). For SMase, we first showed that the enzyme preferably attacks SM in the LE state of the monolayers (Fanani and Maggio, 1997), which was recently found also in bilayer vesicle systems (Ruiz-Arguello et al., 2002), indicating that the phosphohydrolytic reaction preferably proceeds into the LE-phase domain.

In Fig. 3, *a* and *b*, we observe that during the first phase of the enzymatic reaction (until the end of the lag time, t = 2.7 min in Fig. 3 *a*), the number of Cer-enriched domains (lateral defects) increases rapidly until it reaches a plateau. This event marks a first structural threshold point for the transduction of the local catalytic process to the supramolecular mesoscopic level and causes a topographically mediated switch on to a constant rate of the enzymatic activity. When the pseudo-zero-order kinetic activity begins (at t = 2.7 min; Fig. 3 *a*), practically all interfacial-activated SMase is associated irreversibly with the interface (Fanani and Maggio, 2000). This period of the kinetic reaction correlates with the topographic observation that the number of dark domains remains unaltered while growing in size (Fig. 3 *a*).

When the enzymatically generated Cer reaches a proportion of ~70 mol %, a second structural threshold point marks the beginning of the switch-off phase of the enzymatic reaction. At this point the LE phase is disconnected by the percolation of the condensed phase (Fig. 2, *e* and *f*). Concomitantly, the rate of activity departs from the constant-velocity kinetics and the reaction gradually halts. This event implies an abrupt decrease of the amount of lateral domain-domain interfaces (Fig. 3 *b*). As shown previously, the effect of Cer at the interface is to decrease the rate of steady-state catalysis, but it does not impair (it actually favors) the interfacial association and activation of the enzyme (Fanani and Maggio, 1998, 2000). In liposomes, on the other hand, surface defects introduced by gel- and fluid-domain borders near the transition temperature were reported to maximize lag times of SMase (Ruiz-Arguello et al., 2002). Therefore, it is likely that the enzyme associated with the interface becomes impaired to diffuse freely and to continue degrading the LE phase of the substrate (increasingly disconnected because of percolation of the condensed Cer-enriched phase) along the two-dimensional surface. The concept of percolation as a regulator of an enzyme activity (percoregulation) was first suggested from studies of pancreatic lipase activity (Muderhwa and Brockman, 1992). Also, computer simulation suggested a strong influence of the percolation process on two-dimensional enzymatic reaction in a fluid-condensed lipid membrane system (Melo et al., 1992). Our results support the concepts by which the surface topography, through phase connection-disconnection of substrate-enriched or substrate-depleted domains, can dynamically regulate lipolytic activity.

In summary, our present results offer a clear real-time visualization of the close correlation and inter-linkage between kinetic features of SMase and the topographical changes of the substrate-containing surface. In addition, our work points out a transduction of information content between the local molecular level of substrate transformation and the long-range surface organization. In turn, the latter exerts a concerted modulatory influence on the initiation, progression, and halting of the interfacial reaction, establishing bidirectional communication between enzyme activity and interfacial topography. This long-range transfer of information may constitute a generic mechanism for surface-mediated communication between events that underlie the function of amphitropic proteins transducing biochemical and structural information in biomembranes.

The present work was supported by Secretaria de Ciencia y Técnica—Universidad Nacional de Córdoba, Consejo Nacional de Investigaciones Científicas y Técnicas, and Fondo para la Investigación Científica y Tecnológica. S.H. is a Feodor-Lynen-Fellow of the Alexander v. Humboldt Foundation and a postdoctoral Fellow of CONICET. Currently, B.M. is Principal Investigator of CONICET, Argentina.

REFERENCES

Bell, J. D., M. Burnside, J. A. Owen, M. L. Royall, and M. L. Baker. 1996. Relationships between bilayer structure and phospholipase A_2 activity: interactions among temperature, diacylglycerol, lysolecithin, palmitic acid, and dipalmitoylphosphatidylcholine. *Biochemistry.* 35:4945–4955.

Berg, O. G., J. Rogers, B. Z. Yu, J. Yao, L. S. Romsted, and M. K. Jain. 1997. Thermodynamic and kinetic basis of interfacial activation: resolution of binding and allosteric effects on pancreatic phospholipase A_2 at zwitterionic interfaces. *Biochemistry.* 36:14512–14530.

Bianco, I. D., G. D. Fidelio, R. K. Yu, and B. Maggio. 1991. Degradation of dilauroylphosphatidylcholine by phospholipase A_2 in monolayers containing glycosphingolipids. *Biochemistry.* 30:1709–1714.

Bianco, I. D., G. D. Fidelio, R. K. Yu, and B. Maggio. 1992. Concerted modulation by myelin basic protein and sulfatide of the activity of phospholipase A_2 against phospholipid monolayers. *Biochemistry.* 31: 2636–2642.

Boguslavsky, V., M. Rebecchi, A. J. Morris, D. Y. Jhon, S. G. Rhee, and S. McLaughlin. 1994. Effect of monolayer surface pressure on the activities of phosphoinositide-specific phospholipase C-beta 1, -gamma 1, and -delta 1. *Biochemistry.* 33:3032–3037.

Burack, W. R., Q. Yuan, and R. L. Biltonen. 1993. Role of lateral phase separation in the modulation of phospholipase A_2 activity. *Biochemistry.* 32:583–589.

Carrer, D. C., and B. Maggio. 1999. Phase behavior and molecular interactions in mixtures of ceramide with dipalmitoylphosphatidylcholine. *J. Lipid Res.* 40:1978–1989.

Ellison, E. H., and F. J. Castellino. 1997. Adsorption of bovine prothrombin to spread phospholipid monolayers. *Biophys. J.* 72:2605–2615.

Exton, J. H. 1994. Phosphatidylcholine breakdown and signal transduction. *Biochim. Biophys. Acta.* 1212:26–42.

Fanani, M. L., and B. Maggio. 1997. Mutual modulation of sphingomyelinase and phospholipase A_2 activities against mixed lipid monolayers by their lipid intermediates and glycosphingolipids. *Mol. Membr. Biol.* 14:25–29.

Fanani, M. L., and B. Maggio. 1998. Surface pressure-dependent cross-modulation of sphingomyelinase and phospholipase A_2 in monolayers. *Lipids.* 33:1079–1087.

Fanani, M. L., and B. Maggio. 2000. Kinetic steps for the hydrolysis of sphingomyelin by *Bacillus cereus* sphingomyelinase in lipid monolayers. *J. Lipid. Res.* 41: 1832–1840.

Freeman, H. 1970. Boundery encoding and processing. *In* Picture Processing and Psychopictorics. B. S. Lipkin and A. Rosenfeld, editors. Academic Press, New York. 241–266.

Grainger, D. W., A. Reichert, H. Ringsdorf, and C. Salesse. 1990. Hydrolytic action of phospholipase A_2 in monolayers in the phase transition region: direct observation of enzyme domain formation using fluorescence microscopy. *Biochim. Biophys. Acta.* 1023:365–379.

Hannun, Y. A., and C. Luberto. 2000. Ceramide in the eukaryotic stress response. *Trends Cell Biol.* 10:73–80.

Holopainen, J. M., M. I. Angelova, and P. K. Kinnunen. 2000. Vectorial budding of vesicles by asymmetrical enzymatic formation of ceramide in giant liposomes. *Biophys. J.* 78:830–838.

Holopainen, J. M., J. Y. Lehtonen, and P. K. Kinnunen. 1997. Lipid microdomains in dimyristoylphosphatidylcholine-ceramide liposomes. *Chem Phys. Lipids.* 88:1–13.

Holopainen, J. M., M. Subramanian, and P. K. Kinnunen. 1998. Sphingomyelinase induces lipid microdomain formation in a fluid phosphatidylcholine/sphingomyelin membrane. *Biochemistry.* 37: 17562–17570.

Honger, T., K. Jorgensen, R. L. Biltonen, and O. G. Mouritsen. 1996. Systematic relationship between phospholipase A_2 activity and dynamic lipid bilayer microheterogeneity. *Biochemistry.* 35:9003–9006.

Honger, T., K. Jorgensen, D. Stokes, R. L. Biltonen, and O. G. Mouritsen. 1997. Phospholipase A_2 activity and physical properties of lipid-bilayer substrates. *Methods Enzymol.* 286:168–190.

Huang, H. W., E. M. Goldberg, and R. Zidovetzki. 1999. Ceramides modulate protein kinase C activity and perturb the structure of phosphatidylcholine/phosphatidylserine bilayers. *Biophys. J.* 77:1489–1497.

Jain, M. K., J. Rogers, D. V. Jahagirdar, J. F. Marecek, and F. Ramirez. 1986. Kinetics of interfacial catalysis by phospholipase A_2 in intravesicle scooting mode, and heterofusion of anionic and zwitterionic vesicles. *Biochim. Biophys. Acta.* 860:435–447.

Kinnunen, P. K., A. Koiv, J. Y. Lehtonen, M. Rytomaa, and P. Mustonen. 1994. Lipid dynamics and peripheral interactions of proteins with membrane surfaces. *Chem. Phys. Lipids.* 73:181–207.

Maggio, B. 1996. Control by ganglioside GD1a of phospholipase A_2 activity through modulation of the lamellar-hexagonal (HII) phase transition. *Mol. Membr. Biol.* 13:109–112.

Maggio, B. 1999. Modulation of phospholipase A_2 by electrostatic fields and dipole potential of glycosphingolipids in monolayers. *J. Lipid. Res.* 40:930–939.

Maggio, B., I. D. Bianco, G. G. Montich, G. D. Fidelio, and R. K. Yu. 1994. Regulation by gangliosides and sulfatides of phospholipase A_2 activity against dipalmitoyl- and dilauroylphosphatidylcholine in small unilamellar bilayer vesicles and mixed monolayers. *Biochim. Biophys. Acta.* 1190:137–148.

Melo, E. C., I. M. Lourtie, M. B. Sankaram, T. E. Thompson, and W. L. Vaz. 1992. Effects of domain connection and disconnection on the yields of in-plane bimolecular reactions in membranes. *Biophys. J.* 63:1506–1512.

Montes, L. R., M. B. Ruiz-Arguello, F. M. Goni, and A. Alonso. 2002. Membrane restructuring via ceramide results in enhanced solute efflux. *J. Biol. Chem.* 277:11788–11794.

Muderhwa, J. M., and H. L. Brockman. 1992. Lateral lipid distribution is a major regulator of lipase activity: implications for lipid-mediated signal transduction. *J. Biol. Chem.* 267:24184–24192.

Op den Kamp, J. A. F., M. T. Kawerz, and L. L. M. van Deenen. 1975. Action of pancreatic phospholipase A_2 on phosphatidylcholine bilayers in different physical states. *Biochim. Biophys. Acta.* 406:169–177.

Ransac, S., H. Moreau, C. Riviere, and R. Verger. 1991. Monolayer techniques for studying phospholipase kinetics. *Methods Enzymol.* 197:49–65.

Roberts, M. F. 1996. Phospholipases: structural and functional motifs for working at an interface. *FASEB J.* 10:1159–1172.

Ruiz-Arguello, M. B., G. Basanez, F. M. Goni, and A. Alonso. 1996. Different effects of enzyme-generated ceramides and diacylglycerols in phospholipid membrane fusion and leakage. *J. Biol. Chem.* 271: 26616–26621.

Ruiz-Arguello, M. B., M. P. Veiga, J. L. Arrondo, F. M. Goni, and A. Alonso. 2002. Sphingomyelinase cleavage of sphingomyelin in pure and mixed lipid membranes: influence of the physical state of the sphingolipid. *Chem. Phys. Lipids.* 114:11–20.

Souvignet, C., J. M. Pelosin, S. Daniel, E. M. Chambaz, S. Ransac, and R. Verger. 1991. Activation of protein kinase C in lipid monolayers. *J. Biol. Chem.* 266:40–44.

Spink, C. H., M. D. Yeager, and G. W. Feigenson. 1990. Partitioning behavior of indocarbocyanine probes between coexisting gel and fluid phases in model membranes. *Biochim. Biophys. Acta.* 1023:25–33.

Sugar, I. P., N. K. Mizuno, M. M. Momsen, and H. L. Brockman. 2001. Lipid lateral organization in fluid interfaces controls the rate of colipase association. *Biophys. J.* 81:3387–3397.

Tepper, A. D., P. Ruurs, T. Wiedmer, P. J. Sims, J. Borst, and W. J. van Blitterswijk. 2000. Sphingomyelin hydrolysis to ceramide during the execution phase of apoptosis results from phospholipid scrambling and alters cell-surface morphology. *J. Cell Biol.* 150:155–164.

Volwerk, J. J., E. Filthuth, O. H. Griffith, and M. K. Jain. 1994. Phosphatidylinositol-specific phospholipase C from *Bacillus cereus* at the lipid-water interface: interfacial binding, catalysis, and activation. *Biochemistry.* 33:3464–3474.

Vossepoel, A. M., and A. W. M. Smeulders. 1982. Vector code probabilities and metrication error in the presentation of straight lines of finite lenght. *Comput. Graph. Image Process.* 20:347–364.

Wakelam, M. J., T. R. Pettitt, P. Kaur, C. P. Briscoe, A. Stewart, A. Paul, A. Paterson, M. J. Cross, S. D. Gardner, and S. Currie. 1993. Phosphatidylcholine hydrolysis: a multiple messenger generating system. *Adv Second Messenger Phosphoprotein Res.* 28:73–80.